

Imaging of the Shell Galaxies NGC 474 and NGC 7600, and Implications for their Formation

A. J. Turnbull,¹ \star T. J. Bridges² \dagger D. Carter³ \ddagger

¹*Department of Physical Sciences, University of Hertfordshire, Hatfield, College Lane, AL10 9AB, UK.*

²*Institute of Astronomy, Madingley Road, Cambridge, CB3 0E3, UK.*

Current address: Anglo-Australian Observatory, PO Box 296, Epping, NSW 1710, Australia.

³*Liverpool John Moores University, Astrophysics Research Institute, Twelve Quays House, Egerton Wharf, Birkenhead, L41 1LD*

29 August 2018

ABSTRACT

We present photometric observations of two shell galaxies, NGC 474 and NGC 7600. We examine the photometric colours and surface brightnesses of the shells and their host galaxies, and the isophotal parameters of each galaxy. In the case of NGC 474, we find that the shell formation is consistent with a merger origin although it is possible that the close companion NGC 470 is contributing to the shell system via mass transfer. NGC 7600 exhibits shell geometry and colours which also favour a merger origin.

Key words: galaxies: NGC 474, NGC 7600 - galaxies: evolution mechanisms - galaxies: mergers, weak interactions - galaxies: shell galaxies - galaxies: photometry

1 INTRODUCTION

In recent years it has become clear that elliptical galaxies are host to much fine structure. Perhaps the most dramatic fine structures observed are the edge-brightened arcs of stars surrounding and existing within the envelopes of some ellipticals. Originally classified as peculiar galaxies by Arp (1966), but later rediscovered and renamed ‘shell galaxies’ by Malin & Carter (1980), the exact nature and origin of these features still remains unclear.

The publication of Malin and Carter’s (1983) catalogue of 137 shell galaxies, found in the SRC/ESO Southern Sky Survey by eye, showed that about 17% of field ellipticals were surrounded by shells. Seitzer & Schweizer (1990) examined 74 elliptical and SO galaxies, north of $\delta = -15$ deg, brighter than $B_T = 13.5$, and nearby ($cz > 4000 \text{ km s}^{-1}$). They found shells (referred to by Schweizer as ripples, but the name is interchangeable) in more than half of the field ellipticals and in one third of the field SOs. All found the frequency of shells in spirals to be almost negligible. Clearly shells are common in elliptical and SO galaxies. Shell formation and evolution needs to be understood if a complete picture of the formation and evolution of the galaxies they inhabit is to be obtained.

A variety of models have been proposed to form shells (see reviews by Prieur 1990 and Carter 1998). In the minor

merger models (Quinn 1984; Dupraz & Combes 1986; Hernquist & Quinn 1988, 1989) shells are formed from the stars of the secondary galaxy, which merges within the primary. The shells are a result of the phase wrapping (low orbital angular momentum encounters) or spatial wrapping (high orbital angular momentum encounters) of stars belonging to the secondary. The nature of the secondary can also affect the resulting shell system. Not surprisingly then, combining the small cross section for nearly radial encounters with the many types of accretion candidates leads to a wide variety of observed shell morphologies. Heisler & White (1990) pointed out the shortcomings of the three body approach, and used an accretion scenario to study the effect of tidal disruption on the secondary. They found that although the positions of the shells can be reproduced using test particles, in order to accurately reproduce the population of the shells, a self-consistent treatment of the disruption is essential. Dynamical friction against the primary galaxy is another important ingredient, and is believed to allow shells to be produced deep within the potential well. Dupraz & Combes (1987) investigated this analytically. They proposed that the stars least tightly bound to the companion (probably a large fraction of its mass) are pulled away by tidal forces during the first passage close to the main galaxy centre. Afterwards, the surviving companion is braked by friction as it orbits through the galaxy. More stars are ‘peeled’ by tidal forces launched with continuously lower and lower energies. The innermost shells develop at the end, when merging is almost complete.

Whether major disk-disk mergers can also form shells

\star Email: ajt@star.herts.ac.uk

\dagger Email: tjb@aoep.aao.gov.au

\ddagger Email: dxc@astro.livjm.ac.uk

was asked by Schweizer (1980). Hernquist & Spergel (1992) reproduced shell-like structures from such a scenario and Hibbard & Mihos (1995) carried out major merger modelling of NGC 7252 and found that infalling tidal material may be able to create shells; however the simulation was not evolved to this latter stage. The discovery by Balcells (1997) of two very faint, opposed tidal tails, usually considered as a signature of a disk-disk merger, in the shell elliptical NGC 3656 lends some weight to the theory.

Thomson & Wright (1990) put forward a weak interaction model (WIM) as an alternative to the above merger models. The shells are produced from a one-armed spiral density wave induced within a dynamically cold ‘thick disk’ component of the primary galaxy during a fly-by interaction (not a merger) with a secondary companion; the shell-forming stars are initially on circular but not co-planar orbits. Although hot systems such as ellipticals would not be expected to contain such a population of stars on circular orbits, the effectiveness of the test particle model in reproducing so efficiently the shell distributions of NGC 3923 and 0422-476, particularly the inner shells (Thomson 1991), lends credence to the WIM. However, Carter, Thomson & Hau (1998) have recently reported minor axis rotation in NGC 3923, which implies that the underlying potential is in fact prolate. Together with the high velocity dispersion of the galaxy, this argues against the existence of a thick disk as required by the WIM. Carter, Thomson & Hau (1998) include a full discussion on these points.

Photometry offers a simple yet effective way of constraining models of shell formation. Assuming that no significant star formation is induced by the one-armed spiral density wave, a natural prediction of the WIM is that the shell colours should follow the colour gradient of the host galaxy. Accretion of a cold, disk galaxy in its early stages of merging should show a marked colour difference between the red host elliptical and the bluer companion. As the disk ages the colours will redden and the colour difference will be less pronounced. Other secondary candidates are low mass elliptical galaxies, which should still show a slight difference in colour as low mass elliptical galaxies are bluer on average than larger E type galaxies (Visvantha & Sandage 1977).

Previous photometric studies of shell galaxies (Carter, Allen & Malin 1982; Fort et al 1986; Schombert & Wallin 1987; Forbes et al 1995) have in general shown that the shells are similar in colour or slightly bluer than the underlying galaxy, although uncertainties in the shell colours and geometry are large. The motivation of this study is to provide high signal to noise data capable of allowing clear distinctions to be drawn between formation models, and also allowing us to learn more about the stellar population(s) the shells contain.

The surface brightness of the shells, when compared to the underlying galaxy, should provide a further test of the models. In the WIM the shells are a density wave excited in a component of the galaxy, and will be an approximately constant fraction of the surface brightness of this component. It is more difficult to predict the expected distribution in a merger scenario for reasons already mentioned. Through their investigation, Dupraz & Combes (1987) suggested that the outer shells should contain the highest surface brightness. It is difficult to know how to interpret galaxy isophotal data. Bender et al (1988), Bender (1997) and references

therein used the fourth cosine term (B_4) in the Fourier expansion of the azimuthal variation to quantify the isophotal deviations from pure ellipses. It is thought that pointy isophotes (positive B_4) are associated with discs (Nieto et al 1991) whereas galaxies with box-shaped isophotes (negative B_4) are thought to have been produced by a merger or interaction (Binney & Petrou 1985, Bender 1990). Shells are expected to produce boxy isophotes as they follow isopotential not isodensity surfaces and isopotentials are always rounder (Dupraz & Combes 1986). It is interesting to ask whether the correlations between boxiness and other evidence for interactions can be entirely explained by the presence of shells as suggested by Forbes & Thomson (1992). Changes in the semi-major axis position angle with radius can suggest triaxiality.

We present $B - R$ colours and surface brightnesses for NGC 474 and NGC 7600, and their shells. We also present an isophotal analysis for each galaxy, as well as an investigation into associated fine structure and environment. Observations are discussed in §2, data reduction in §3 and results in §4. We analyse our findings in the context of the shell formation models in §5 and summarise our conclusions in §6.

2 OBSERVATIONS

Broadband B images of NGC 474 were taken at the prime focus of the 4.2m William Herschel Telescope in December 1994. We used a 1024×1024 Tektronix thinned CCD, giving a field of 7.2×7.2 arcminutes with 0.42 arcsec/pixel. NGC 474 fit comfortably onto the chip, although there is some slight clipping of the outer shell, lying 190 arcseconds from the galaxy centre. Broadband R and narrowband $H\alpha$ images of NGC 474 and B, R for NGC 7600 were obtained at the 2.5m Isaac Newton Telescope in November 1996. Again a Tektronix CCD was used at prime focus, giving a field of view of 11.5×10.6 arcminutes and an image scale of 0.59 arcsec/pixel. The seeing was ~ 1.5 arcsec for each run and filter. The total integration times are listed in Table 1. Although included in the table, the $H\alpha$ image is not presented in this paper. When a scaled R -band image was subtracted from the $H\alpha$ image, no traces of $H\alpha$ emission were visible.

3 DATA REDUCTION

Standard IRAF data reduction techniques were used. After debiasing, our images were divided by a normalised flat field in the appropriate pass band, each obtained from a number of exposures taken during twilight. Each passband’s individual images, aligned to within a fraction of a pixel using IMALIGN, were then combined using IMCOMBINE. This employed a median algorithm, scaled to the mode and was very efficient at removing the cosmic rays. The seeing was ~ 1.5 arcsec for all images, and this as well as the accuracy of the aligning was checked by examining the FWHM of several stars in the frame before and after combining. When aligning the combined images with each other the same procedure was used as before except in the case of NGC 474, where as mentioned earlier the B and R images were taken on different telescopes. It was therefore necessary to correct

Table 1. Summary of the Observations. Positions, recession velocities, and B_T magnitudes are taken from the NASA/IPAC Extragalactic Database (NED).

Galaxy	Filter	RA (1950)	Dec (1950)	V_r (km/sec)	B_T	Integration Time (sec)	Telescope
NGC 474	R	$01^h 17^m 31.7^s$	$+3^\circ 9' 17''$	2372	12.37	2700	INT
NGC 474	$H\alpha$					9000	INT
NGC 474	B					3600	WHT
NGC 7600	R	$23^h 16^m 18.2^s$	$-7^\circ 51' 11''$	3436	12.91	2700	INT
NGC 7600	B					5400	INT

Table 2. Calibrated zero points.

Galaxy and Filter	Zero Point	rms ($\frac{\sigma}{\sqrt{N}}$)
NGC 474 R	25.081	0.02
NGC 474 B	25.768	0.01
NGC 7600 R	24.895	0.01
NGC 7600 B	25.175	0.01

for different chip scales and pixel sizes. The packages GEOMAP and GEOTRAN were used for this. GEOMAP computes the transformation required to map the coordinate system of the reference image to that of the input image, using over a dozen stars common to each frame, while GEOTRAN performs the transformation. Total flux was conserved and the accuracy checked as before.

3.1 Photometric Calibration

Calibration was performed using the PHOT package in IRAF. The zero point for each night was found using a number of Landolt (1992) standard stars taken throughout the night; it was found that colour terms were not required. Mean extinction values provided by the Carlsberg Meridian Telescope were used to correct for atmospheric extinction, based on many observations of standard stars throughout the night. Although small, galactic extinction has been corrected for using the interstellar extinction law given by Rieke & Lebofsky (1985). The zero point was calculated for an individual galaxy frame and then recalibrated to the combined galaxy frame. The resulting zero points of the combined galaxy frames are displayed in Table 2. The difference in R zero points between NGC 474 and NGC 7600 is due to the different scaling used to produce the final composite galaxy images.

To test the reliability of our calibration, we have compared the surface brightness profiles of our galaxies with those published by other authors. Shown in Figure 1 is the B surface brightness profile for NGC 474 taken from Schombert & Wallin (1987). Our results, overplotted as filled circles, are in very good agreement. For NGC 7600 we have compared our data with that of Penereiro et al., (1994). Shown in Figure 2 as open circles with error bars is the surface brightness of NGC 7600 transformed from the Gunn r filter as deduced by Penereiro et al into our Kron-Cousins R ; our data are overplotted as filled circles, the symbol size being of the order of our error. We used the transformation given by Jorgensen (1994) to convert from the Gunn system to our Kron-Cousins photometric system. There is a zero-

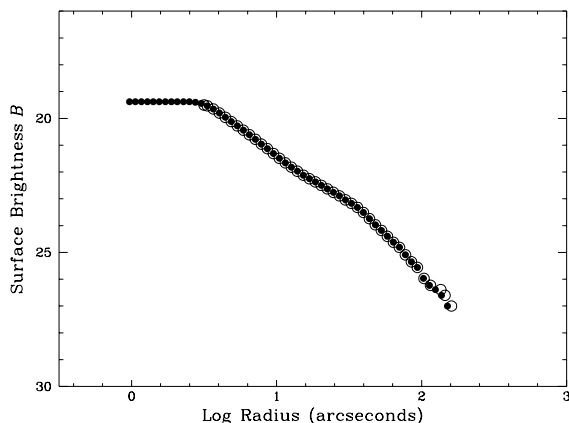


Figure 1. Comparison of NGC 474 B photometric calibration with Schombert & Wallin (1987). Our data are overplotted as filled circles.

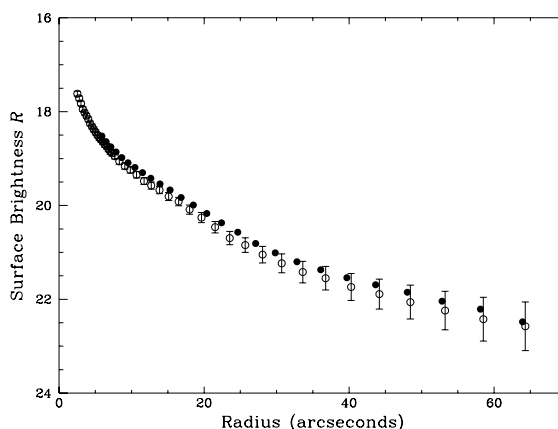


Figure 2. Comparison of NGC 7600 R photometric calibration with Penereiro et al., (1994) converted from Gunn r to Kron-Cousins R . Our data are overplotted as filled circles.

point difference of ~ 0.2 mag between our photometry and that of Penereiro et al., but the agreement is satisfactory.

3.2 Modelling the Underlying Galaxy

Apart from rare cases such as the outer shells of NGC 474, shells are faint structures and difficult to detect since they are superimposed upon the bright background of the galaxy. The galaxy signal also contaminates the signal from a shell.

It is necessary therefore to produce and subtract off a model of the underlying galaxy. First, the contribution of the sky background was estimated from the mean value of several 10×10 pixel boxes placed in regions well away from the galaxy. Our isophotal analysis made use of the ELLIPSE task within STSDAS[§], which is based on the method described in detail by Jedrzejewski (1987). We used a similar technique of ellipse fitting as that described by Forbes & Thomson (1992). In the case of NGC 474, where the bright shells significantly affect the galaxy isophotes, a first model was run with the centre, position angle and ellipticity allowed to vary. A second model was then run with the central position fixed at the value found from the first run. The brightest 10% of pixels in each ellipse were excluded, to avoid the brightest points in the shells. NGC 7600 was found to produce a residual image of comparable quality whether or not the parameters were fixed, and for this galaxy all parameters were allowed to vary and no clipping was used.

3.3 Aperture Photometry of Shells

First we identified the regions of the residual map where shells are present. A 10×10 pixel box was placed on the shell, being careful to avoid foreground stars, globular clusters and any other unwanted features. On either side of shell the task was repeated in order to deduce the local sky+galaxy background. The procedure was repeated along the shell, the number of times depending upon the size of shells. Typically this ranged from 5 to 15 independent boxes. The corresponding shell surface brightness (SB) was thus deduced for each aperture using the formula:

$$SB = -2.5 * \log\left(\frac{counts}{itime}\right) + m0 \quad (1)$$

where *counts* are per square arcsecond, *itime* is the exposure time in seconds, and *m0* the zero point for that filter. This was repeated for the other filter using identical positions, and the colour indices calculated. After checking for possible colour gradients, the mean value for the shell was determined. Any remaining spurious features were re-examined, and those apertures lying further than two σ away from the mean were rejected and the mean recalculated. The final shell surface brightnesses were calculated by averaging the surface brightnesses calculated for each aperture along the shell.

3.3.1 Error Analysis

The low surface brightness of the shells and the high signal from the galaxy and sky lead to some uncertainty in the final shell magnitude due to random measurement errors. We adopted the following procedure to calculate this uncertainty. The value σ_D was calculated for one of the band passes:

$$\sigma_D = \sqrt{\sigma_{shell}^2 + \frac{\sigma_{sky1+galaxy1}^2 + \sigma_{sky2+galaxy2}^2}{2}} \quad (2)$$

[§] The Space Telescope Science Data Analysis System STSDAS is distributed by the Space Telescope Science Institute.

Table 3. NGC 474 shell parameters. For details see text.

Shell Radius (arcseconds)	Brightness (R mag/arcsec ²)	$B - R$
202	24.67	1.00 \pm 0.05
192	24.98	0.91 \pm 0.05
140	25.46	1.21 \pm 0.08
121	25.61	1.10 \pm 0.09
100	24.92	1.24 \pm 0.06
74	25.29	1.34 \pm 0.08
72	24.95	1.33 \pm 0.06
63	25.45	1.16 \pm 0.08
55	24.53	1.21 \pm 0.05
50	24.91	1.44 \pm 0.08

These are the associated standard deviations of the values returned from the 10×10 pixel box placed on and to each side of the shell. The procedure was repeated for all apertures along the shell in that filter and the standard error for the whole shell calculated using (assuming we are in the R Band):

$$\sigma_R = \sqrt{\sum_{i=1}^N \frac{\left(\frac{\sigma_{D_i}}{\sqrt{n}}\right)^2}{N}} \quad (3)$$

Here, N is the number of apertures along the shell, which was typically no less than five and reached fourteen for some of NGC 474's larger shells, and n is the number of pixels in the aperture which is 100 in our case. The above process was repeated for the B filter and the total error calculated as:

$$\sigma_{B-R} = \sqrt{\left(\frac{\sigma_B}{\bar{n}_B}\right)^2 + \left(\frac{\sigma_R}{\bar{n}_R}\right)^2 + (0.01)^2 + (0.02)^2} \quad (4)$$

\bar{n}_R and \bar{n}_B are the average counts for the shell in R and B respectively. We have adopted zero-point errors of 0.01 and 0.02 for B and R respectively, for NGC 474 (see Table 2). For the NGC 474 shell at 202 arcseconds radius, we calculated $\sigma_{B-R} = 0.05$. We further calculated that this shell had an average $B - R$ of 1.00 leading to a final value of 1.00 ± 0.05 . We believe ± 0.05 is a realistic error when obtaining shell colours based on the techniques described in this paper.

4 RESULTS

In Tables 3 and 4 we list, for NGC 474 and NGC 7600 respectively, the average radius, surface brightness, and $B - R$ colour of each shell. We also present plots of $B - R$ and surface brightness for the shells and host galaxies in this section.

4.1 $B - R$, Surface Brightness, and Isophotal Parameters

4.1.1 NGC 474

In Figure 5a we plot R surface brightness versus $r^{1/4}$ for NGC 474. Figures 5b,6ab contain the isophote data obtained for NGC 474, namely ellipticity, B_4 (the fourth cosine term



Figure 3. *R* band galaxy subtracted image of NGC 474. North is up and East is to the left. The eastern-most shell is 202 arcsec from the galaxy centre. NGC 470 is located just off the frame, ~ 300 arcsec West. The field of view is $9'$.

in the Fourier expansion of the azimuthal variation from pure ellipse), and position angle plotted against radius. The position angle of the semi-major axis and the ellipticity of NGC 474 change quite dramatically with radius. The $\cos B_4$ term shows significant scatter and prevents conclusions from being drawn.

Figure 7a shows the $B - R$ profiles for NGC 474 and its shells. The galaxy signal falls off to background dominated values after 150 arcseconds and these points are not included. The shell $B - R$ colours seem to follow those of the galaxy; this is more uncertain for the two outer-most points, since this involves an extrapolation of the galaxy colours to larger radius. It could also be argued that the colours of the *inner* shells are constant with radius, within the errors;

the two outer-most shells are significantly bluer than the rest. The R surface brightness of NGC 474 and its shells are plotted in Figure 7b. The shell surface brightness appears to remain constant with radius, and below that of the galaxy within 100 arcsec. The outer shells, however, appear to be bluer and it would be useful to measure the galaxy surface brightness out to this radius. The two outer-most shells also have a higher surface brightness than most of the inner shells, though not significantly so. The fact that the shell surface brightness does not follow that of the galaxy argues strongly against the WIM; we return to this point in Section 5.

Despite clipping, the question remains as to whether some shell light is included in the model images. The resid-



Figure 4. *R* band galaxy subtracted image of NGC 7600. North is up and East is to the left. The dark oval shape is an artifact of the subtraction process. The eastern-most shell lies 215 arcsec away from the galaxy centre. The field of view is $9'$.

ual images would then be an underestimate of the true shell light, which if a function of radius, would effect the final shell colours. With no galaxy subtraction, the bright shell at a radius of 202 arcseconds has a $B - R$ of 1.05 ± 0.05 . This value with associated error being obtained using the procedure outlined in section 3.3. From Table 3, we see that this is not a significant change within the errors. This shell has a high surface brightness and is furthest from the galaxy centre, so we believe that a realistic upper limit for the systematic uncertainty in the shell colours introduced by the possible inclusion of shell light in the galaxy model is 0.5 in $B - R$. The effect will be smaller for NGC 7600, which has fainter shells. Despite some scatter in the points, the isophote plots do not seem to show features at the radii of

the shells which is a strong point for proving their exclusion in the model. However, NGC 474 has a large, high surface-brightness shell at a radius of 55 arcseconds. A model run with this shell feature masked out significantly reduced the boxiness at that radius. Specifically the B_4 parameter was reduced from -0.04 to -0.01 with errors of the order ± 0.005 . It would seem this shell is responsible for the observed boxiness. The position angle and ellipticity were unaffected.

4.1.2 NGC 7600

In Figure 8a, we plot the *R* surface brightness versus $r^{1/4}$ for NGC 7600. Figures 8b,9ab plot the isophotal data for NGC

Table 4. NGC 7600 shell parameters. Blank spaces indicate that although a shell was present, it was either dominated by spurious objects or the signal was too low for accurate photometry. For further details see text.

Shell Radius (arcseconds)	Brightness (R mag/arcsec ²)	$B - R$
215	25.76	1.35 ± 0.12
151	24.91	1.35 ± 0.06
118	25.91	1.37 ± 0.15
112	26.36	1.52 ± 0.24
97		
92	26.29	1.60 ± 0.21
79		
76	25.91	1.53 ± 0.18
67		
58	25.05	1.49 ± 0.04
56		
53	25.66	1.46 ± 0.11
49	25.33	1.68 ± 0.13
46		
41		
38		

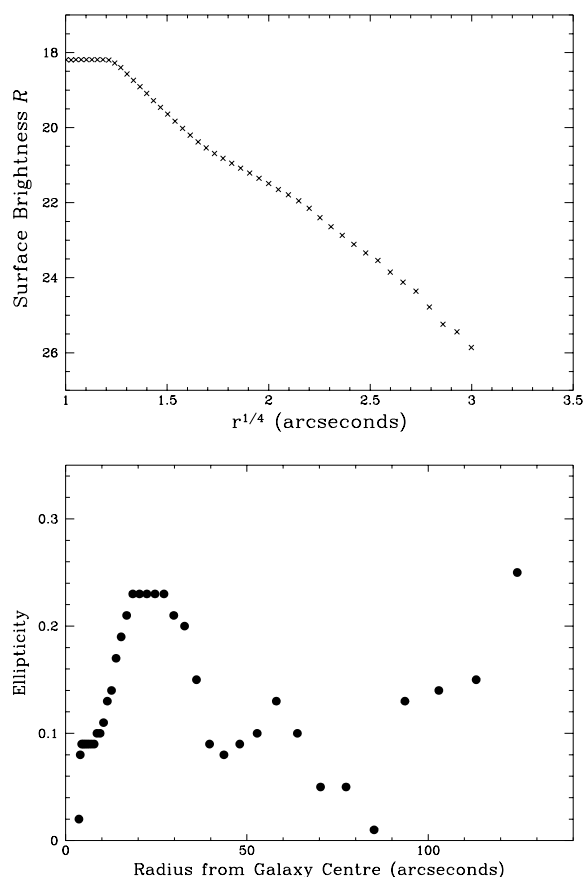


Figure 5. (5a top) NGC 474 R surface brightness versus $r^{1/4}$ and (5b bottom) NGC 474 ellipticity versus radius. The errors are of the order of the symbol size.

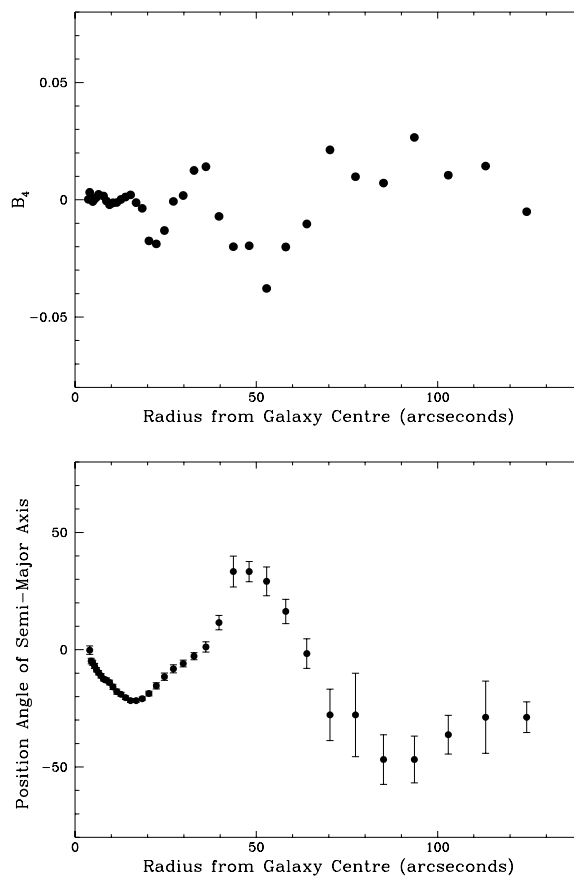


Figure 6. (6a top) NGC 474 $\cos B_4$ term versus radius and (6b bottom) NGC 474 position angle of the semi-major axis versus radius. The errors are of the order of the symbol size in the absence of error bars.

7600. The position angle changes little with radius, while the ellipticity rises sharply within 10 arcsec, and flattens out at ~ 0.55 at larger radius. The $\cos B_4$ term is negative (boxy) at most radii.

Figure 10a shows the $B - R$ for the galaxy and shells. The galaxy $B - R$ is flat over the radius plotted (again, the galaxy signal is dominated by sky after 150 arcseconds and these points are not included). The inner shells have roughly the same colour as the galaxy, while the three outer-most shells are bluer than the galaxy, with $B - R \simeq 1.35$. Given the errors, it could be argued that there is a general trend that the shells become bluer with increasing radius. The shell and galaxy surface brightness are shown in Figure 10b. The shells in NGC 7600 have a surface brightness roughly constant with radius, and do not follow the galaxy surface brightness at all (except for possibly the two outer-most points).

4.2 Associated Fine Structure and Environment

4.2.1 NGC 474

NGC 474 has a peculiar kinematic structure in its core (Balcells, Hau & Carter 1998), with the core rotating about an axis intermediate between photometric major and minor axes. There is also evidence in the rotation curves of

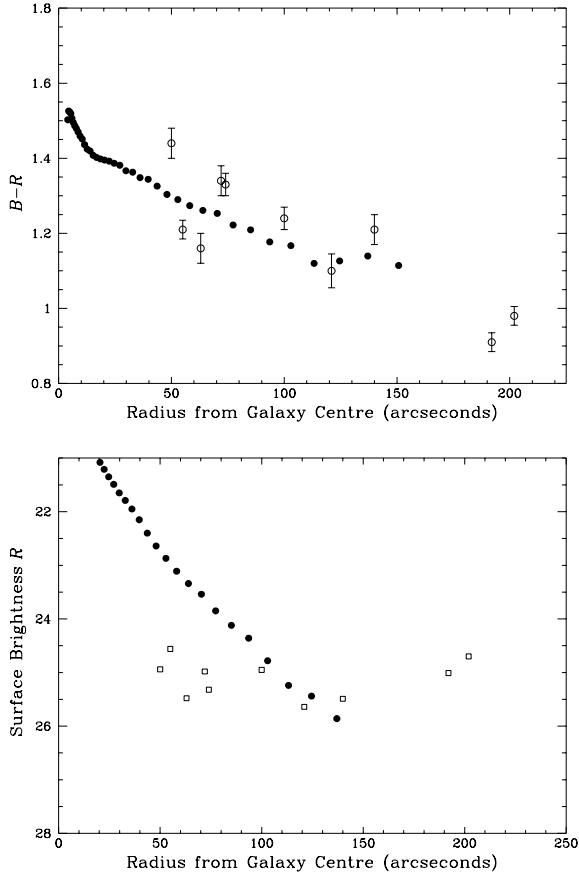


Figure 7. (*7a top*) NGC 474 $B-R$ of the galaxy and shells versus radius and (*7b bottom*) the surface brightness of NGC 474 and shells versus radius. In all cases the galaxy data are represented as filled circles, the error being of the order of the symbol size. The shell data are open circles with error bars.

this galaxy for kinematic shells, of the type also seen in NGC 7626 (Balcells & Carter 1993). The shell system of NGC 474 was classed as a type II by Prieur (1988), meaning that the shells have no preferred orientation around the galaxy. From the residual image in Figure 3 we see that the two outer most shells appear to be linked to each other by a ‘tidal feature’ which crosses the center of the galaxy. NGC 474 is a close partner of the smaller spiral NGC 470. Both have identical recessional velocities and are at a projected separation of 300 arcseconds (60 kpc for $H_0=75$ km/sec/Mpc). NGC 470 is undergoing an intense nuclear starburst and has a weak bar (Freidli et al 1996). It has strong central CO emission whereas NGC 474 is weaker (Sofue et al 1992). The two are linked via an HI tidal bridge, and NGC 470 appears to be in orbit about NGC 474 as the HI mimics a ‘Magellanic stream’ around NGC 474 (Schiminovich et al 1997).

4.2.2 NGC 7600

Dressler & Sandage (1983) studied the kinematics in the central 20 arcsec of NGC 7600. Although the uncertainties are large, the bulge $\frac{v}{\sigma}$ versus ellipticity places NGC 7600 close towards the theoretical line for a prolate elliptical (see their Figure 2). Based on its morphology, especially the ex-

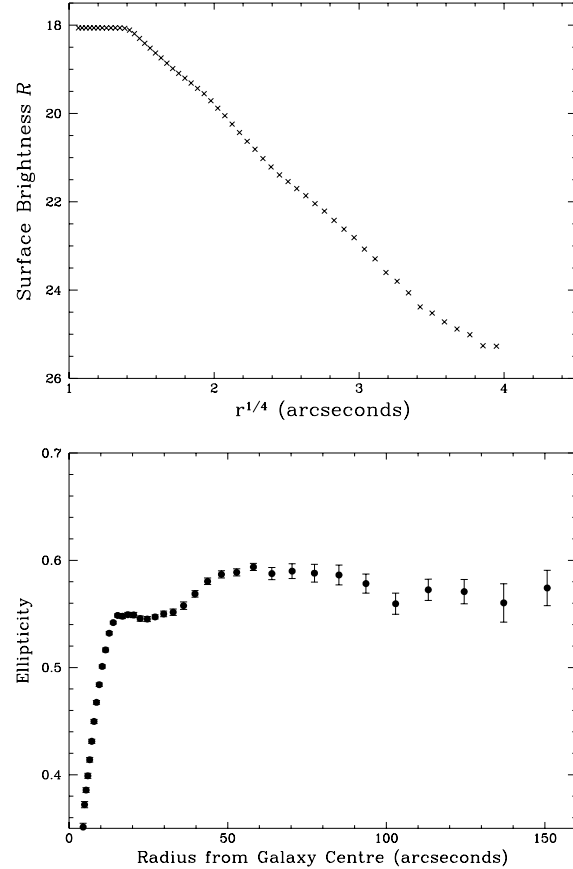


Figure 8. (*8a top*) NGC 7600 R surface brightness versus $r^{1/4}$ and (*8b bottom*) NGC 7600 ellipticity versus radius.

tended envelope, it has been classified as an S0. Dressler & Sandage claim that the low rotation of NGC 7600 implies that it is closer to an elliptical, with its support and flattening arising from a large velocity dispersion. They coined the phrase ‘diskless S0’ to describe NGC 7600 and similar galaxies. Schweizer & Seitzer (1988) noted that the ripples of NGC 7600 interleave with radius, and concluded that they probably arose from an external origin. We give NGC 7600 the classification of type I, based on this interleaving of shells aligned along the major axis. On inspection of the surrounding area, there appears to be no companion to NGC 7600.

5 DISCUSSION

Here we discuss our results in light of models of shell formation.

5.1 NGC 474

Hernquist & Quinn (1988) showed that mass transfer, rather than complete mergers, were also capable of producing shell structures. They also noted that the efficiency of tidal stripping is greatly reduced in retrograde encounters. Longo & de Vaucouleurs (1983) quote a mean outer-disk colour for NGC 470 of $B-V = 0.68$. We transform this to $B-R = 1.00$, ($\frac{\sigma}{v}$) ~ 0.08 based on observations of many disk

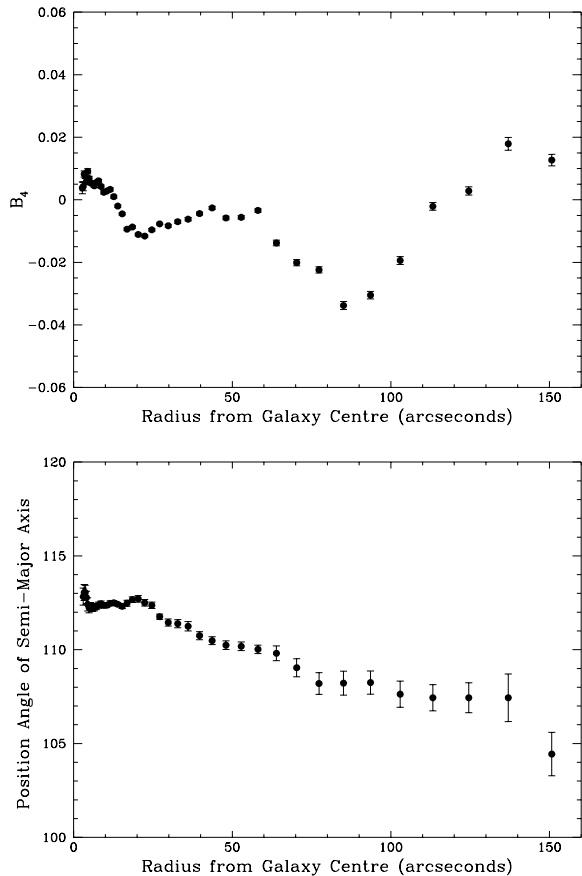


Figure 9. (9a top) NGC 7600 $\cos B_4$ term versus radius and (9b bottom) NGC 7600 position angle of the semi-major axis versus radius.

galaxies in different filters by de Jong (1995). If (some of) the shells of NGC 474 are indeed stripped matter from NGC 470, then we must take into account subsequent passive stellar evolution (which would redden the shells) and also the expected blueing of shells as dust is removed during the interaction. We will assume for the moment that the two processes cancel each other. (It may also be the case, as suggested by the HI maps of the two systems, that NGC 470 is in orbit about NGC 474 and thus periodically replenishes the outer shells; the colours of the (outermost) shells would then also depend on the orbital timescale, further complicating the issue). Within our uncertainties, the two outer-most shells have colours consistent with being stripped matter from NGC 470 ($B - R$ of 0.91 and 0.99). The inner shells however have a mean $B - R$ of 1.27 ± 0.04 , not compatible with the outer-disk colour of NGC 470. The discovery of kinematic shells and a peculiar core deep within the potential well of NGC 474 is important in this context. It is very unlikely that the mass transfer of material could form shells at very small radii, and which would exist for the timescales required. Kinematically-distinct core (KDC) ellipticals have central regions that rotate rapidly, and often in the opposite direction to the stars in the outer parts of the galaxy. KDCs are believed to be result of a merger (Illingworth & Franx 1989), either the accretion of a small secondary (Balcells & Quinn 1990) or a major merger of two nearly equal-mass disk

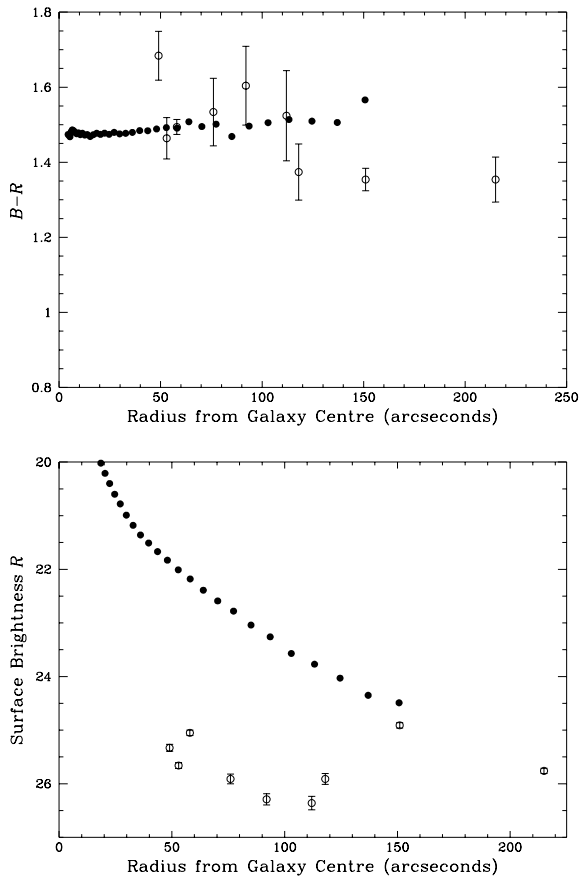


Figure 10. (10a top) NGC 7600 $B - R$ of the galaxy and shells versus radius and (10b bottom) surface brightness of the galaxy and shells versus radius. In all cases the galaxy data are represented as filled circles, the error being of the order of the symbol size. The shell data are open circles with error bars

galaxies (Hernquist & Barnes 1991). Forbes (1992) found that in a sample of galaxies with peculiar cores almost all had shells, implying that shells and KDCs may form in a similar way, namely via mergers (although the role of major mergers in shell formation is poorly understood).

In the WIM (Thomson 1991), the shell system of NGC 474 was formed via a weak interaction with NGC 470. Mass transfer to some degree is also compatible with the WIM, and could explain the origin of the outer shells. The similarity of the galaxy and shell $B - R$ profiles in NGC 474 is in agreement with the WIM, but the fact that the shells' surface brightness does *not* follow that of the galaxy is a very strong (perhaps fatal) argument *against* the WIM. Hau & Thomson (1994) showed how a fly-by interaction can form a decoupled core by spinning up the envelope of the galaxy. How this would effect the thick disk is not known but we would expect it to be heated up thus suppressing shell formation. It seems therefore that in order to produce the peculiar core and the shells a merger would still be needed even in this scenario.

It seems plausible to use an accretion event to explain the inner shells of NGC 474 and the peculiar core kinematics. More speculatively, the two outer-most shells may be the result of mass transfer from NGC 470.

5.2 NGC 7600

With no close companions and no evidence for other peculiar structure apart from the shells, NGC 7600 is a much cleaner system than NGC 474. NGC 7600 is, like NGC 3923, an example of the expected result of a minor merger between a prolate elliptical and a dwarf elliptical on a near radial orbit (Dupraz & Combes 1986). This indeed seems to be consistent with the data. First, the shell system is aligned along the apparent major axis and appears interleaved. Second, although tentative the $B - R$ of the outer shells appear different to the $B - R$ of the galaxy although the inner shells are consistent with the $B - R$ of the galaxy. It is difficult to know whether a gradient exists in the $B - R$ of the shells due to the low surface brightness of the shells coupled with the missing values of some. On balance, however, we believe that the $B - R$ profile and surface brightness of the shells point towards them being formed from the stars of a merged secondary.

6 CONCLUSIONS AND FUTURE WORK

We have presented the first results from our investigation into the photometric colours of shell galaxies. Once reduction and calibration of the rest of the sample is complete we hope to make some statements concerning the generic properties of these galaxies. A key result from the present study of NGC 474 and NGC 7600 is that the shell surface brightness is roughly constant with radius. This is a strong argument against the Weak Interaction Model (Thomson 1991), which predicts that the surface brightness profile of the shells should follow that of the galaxy. Wilkinson et al. (1998/1999) also argue against the WIM from their study of the shell system of 0422-476.

Our hypotheses for the two galaxies is as follows. NGC 474 may have two families of shells. The outer-most shells were possibly formed from tidally liberated material from its interacting companion NGC 470, while the inner shells formed by a minor merger which is now shaping the galaxy's core. For NGC 7600, our results favour shell formation from a merger/accretion of a smaller companion.

Unfortunately, the various formation models, chiefly mergers and the WIM, are not developed enough to allow unique, testable predictions for shell morphologies, surface brightnesses and colours. For instance, the shell colours of NGC 474 and NGC 7600 do not allow us to distinguish between a WIM and a merger model. Detailed numerical simulations of shell formation in the various scenarios, incorporating dynamical friction and realistic treatments of gas and dust, are needed to differentiate between the different models, and to learn more about the progenitors. On the observational side, shell *kinematics* holds considerable promise. For instance, Merrifield & Kuijken (1998) showed that the measurement of shell kinematics in regular, aligned systems provides a means for determining the gravitational potential of their host galaxies out to large radii. Such measurements will become feasible with integral-field spectrographs on 8–10m class telescopes.

7 ACKNOWLEDGEMENTS

AJT would like to thank Bob Thomson for initiating the project and for many helpful ideas and interesting discussions. We would like to thank Jim Collett for contributions to the discussion.

This research has made use of the NASA/IPAC Extragalactic Database (NED) which is operated by the Jet Propulsion Laboratory, California Institute of Technology, under contract with the National Aeronautics and Space Administration.

The Isaac Newton Telescope is operated on the island of La Palma by the Royal Greenwich Observatory in the Spanish Observatorio del Roque de los Muchachos of the Instituto de Astrofísica de Canarias.

8 REFERENCES

- Arp, H. 1966, in *Atlas of Peculiar Galaxies*, Pasadena, California Institute of Technology
- Balcells, M. 1997, ApJ, 486, L87
- Balcells, M., & Carter, D. 1993, Astron. Astrophys, 279, 376
- Bender, R., Dobereiner, S & Mollenhoff, C., 1988. Astr. Astrophys. Suppl, 74, 385
- Bender, R., 1990, in *Dynamics and Interactions of Galaxies*, p.232, ed. R. Wielen (Springer, Berlin)
- Binney, J., & Petrou, M. 1985, MNRAS, 214 449
- Carter, D., preprint for IAU 186, 1997
- Carter, D., Allen, D. A., & Malin, D. F. 1982, Nature, 295, 126
- Carter, D., Thomson, R. C., & Hau, G. K. T. 1998, MNRAS, 294, 182
- de Jong, R. S. 1995, *Thesis*, Groningen, Netherlands.
- Dressler, A., & Sandage, A. 1983, ApJ, 265, 664
- Dupraz, C., & Combes, F. 1986, A&A, 166, 53
- Dupraz, C., & Combes, F. 1987, A&A, 185, L1
- Fort, B. P., Prieur, J-L., Carter, D., Meatheringham, S. J., & Vigroux, L. 1986, ApJ, 306, 110
- Forbes, D. A., Reitzel, D. B., Williger, G. M. 1995, Astron. J, 109(4), 1576
- Forbes, D. A., & Thomson, R. C. 1992, MNRAS, 254, 723
- Friedli, D., Wozniak, H., Rieke, M., Martinet, L., & Bratschi, P. 1996, A&ASupp, 118, 461
- Heisler, J., & White, S. D. M. 1990, MNRAS, 243, 199
- Hibbard, J. E., & Mihos, J. C. 1995, Astron. J, 110, 140
- Hernquist, L., & Quinn, P. J. 1988, ApJ, 331, 682
- Hernquist, L., & Quinn, P. J. 1989, ApJ, bf 342, 1
- Hernquist, L., & Spergel, D. N. 1992, ApJ, 399, L117
- Jedrzejewski, R. I. 1987, MNRAS, 226, 747
- Jorgensen, I. 1994, PASP, 106, 967
- Landolt, A. U., 1992, AJ, 104(1), 340
- Longo, G & de Vaucouleurs, A. 1983, Univ. Tex. Monogr. Astron. No.3
- Malin, D. F., & Carter, D. 1983, ApJ, 274, 534
- Malin, D. F., & Carter, D. 1980, Nature, 285, 643
- Merrifield, M., & Kuijken, K. 1998, MNRAS, 29, 1292
- Nieto, J-L., Bender, R., Arnaud, J., & Surma, P. 1991, Astr. Astrophys, 244, L25
- Penreiro, J. C., de Carvalho, R. R., Djorgovski, S., & Thompson, D. 1994, A&A Supp, 108, 461
- Prieur, J-L., 1988, *Thesis*, Toulouse, (France)

- Prieur, J.-L., 1990, in *Dynamics and Interactions of Galaxies*, p.72, ed. R. Wielen (Springer, Berlin)
- Quinn, P.J. 1984, ApJ, 279, 596
- Schiminovich, D., Van Gorkom, J. H & Van der Hulst, J. M. 1997, IAU S186
- Schombert, J. M., & Wallin, J. F. 1987, AJ, 94(2), 300
- Schweizer, F. 1980, ApJ, 237, 303
- Schweizer, F., & Seitzer, P. 1988, ApJ, 328, 88
- Seitzer, P., & Schweizer, F. 1990, in *Dynamics and Interactions of Galaxies*, p.270, ed. R. Wielen (Springer, Berlin)
- Thomson, R. C., & Wright, A. E. 1990, MNRAS, 247, 122
- Thomson, R.C. 1991, MNRAS, 257, 689
- Visvanathan, N., & Sandage, A. 1977, ApJ, 216, 214
- Wilkinson, A., Prieur, J.-L., Lemoine, R., Carter, D., Malin, D., Sparks, W. B. 1998, preprint